Lattice symmetry applied in transfer-matrix methods for photonic crystals

Lan-Lan Lin, Zhi-Yuan Li, and Kai-Ming Ho

Citation: J. Appl. Phys. **94**, 811 (2003); doi: 10.1063/1.1587011
View online: http://dx.doi.org/10.1063/1.1587011
View Table of Contents: http://jap.aip.org/resource/1/JAPIAU/v94/i2
Published by the American Institute of Physics.

Additional information on J. Appl. Phys.

Journal Homepage: http://jap.aip.org/
Journal Information: http://jap.aip.org/about/about_the_journal
Top downloads: http://jap.aip.org/features/most_downloaded
Information for Authors: http://jap.aip.org/authors

ADVERTISEMENT

Downloaded 09 Apr 2013 to 171.67.34.205. This article is copyrighted as indicated in the abstract. Reuse of AIP content is subject to the terms at: http://jap.aip.org/about/rights_and_permissions

Lattice symmetry applied in transfer-matrix methods for photonic crystals

Lan-Lan Lin, Zhi-Yuan Li,[a] and Kai-Ming Ho
Ames Laboratory and Department of Physics and Astronomy, Iowa State University, Ames, Iowa 50011

(Received 11 November 2002; accepted 2 May 2003)

Transfer-matrix methods have been routinely used to calculate the transmission and reflection spectra of electromagnetic waves propagating through a photonic crystal slab. In this article we show that the intrinsic lattice symmetries within a photonic crystal can be used to reduce numerical computations of the electromagnetic problem. We have employed this lattice-symmetry enhanced transfer-matrix method to handle two-dimensional photonic crystal slabs of square and triangular lattices and three-dimensional layer-by-layer photonic crystal slabs. The calculated transmission spectra agree excellently with the photonic band structures in predicting the photonic band gap positions, indicating the accuracy and efficiency of this proposed approach. © *2003 American Institute of Physics.* [DOI: 10.1063/1.1587011]

I. INTRODUCTION

In recent years there has been increasing interest in photonic crystals due to their potential application in a range of high technology areas such as ultrasmall all-optical or electro-optic integrated circuits.[1–3] As a material with a periodic modulation of the dielectric function, a photonic crystal is characterized by photonic bands and photonic band gaps in its energy spectrum. This energy spectrum can be detected by looking at the transmission and reflection spectra for an external electromagnetic (EM) wave incident on a photonic crystal slab. A frequency range of null transmission and total reflection would correspond to a photonic band gap.

The transmission and reflection spectra are routinely solved by a transfer-matrix method (TMM). Usually, a TMM can be categorized into two classes, depending on what basis functions are used to represent the EM field distribution. In one class of methods, the plane wave functions are utilized due to the periodic nature of a photonic crystal.[4–9] This class of approaches has been developed by people in the grating community in the past several decades. The other class, developed by Pendry and co-workers,[10,11] represents the EM field by values in a number of sampling points in the real space, and approximates Maxwell's equations by finite-difference equations connecting fields in neighboring sampling points. In previous studies, one special feature entitled to a photonic crystal, the intrinsic lattice symmetry, has not been fully appreciated. In this article, we will show that application of these lattice symmetries can not only reduce the numerical computation burden of the TMM, but also improve the efficiency of the method. We will only consider the class of methods adopting the plane wave basis.

This article is arranged as follows. In Sec. II and Appendix A, we give a brief description of the TMM in the plane wave basis. In particular, the numerically stable S-matrix technique is presented, including an important iteration algorithm for a photonic crystal slab. In Sec. III we introduce the lattice symmetry into the conventional TMM, and present some rules governing the transformation of a transfer matrix under lattice translation and rotation operations. In Sec. IV we will apply the lattice-symmetry enhanced TMM to treat several examples of EM waves diffraction by a photonic crystal slab. Some concluding remarks are made in Sec. V.

II. TRANSFER-MATRIX METHOD IN THE PLANE WAVE BASIS

Suppose a plane EM wave is incident from the left hand side on a photonic crystal slab placed in an air background. Let the wave propagate along the z-axis direction, the incident wave vector is $\mathbf{k}_0=(k_{0x},k_{0y},k_{0z})=k_0(\sin\theta\cos\phi,\sin\theta\sin\phi,\cos\theta)$, where k_0 is the wave number, θ and ϕ are the polar and azimuthal angles, respectively, and the electric field amplitude is $\mathbf{E}_0=(E_{0x},E_{0z},E_{0z})$. For the present, we consider a general three-dimensional (3D) photonic crystal slab, corresponding to which we are dealing with the diffraction problem of EM waves by a two-dimensional (2D) grating. The situation of a 2D photonic crystal slab (and thus the diffraction problem of a 1D grating) can be directly derived from the 3D case. Let the primitive lattice $\mathbf{R}$ of the grating in the XY plane has two unit vectors $\mathbf{a}_1$ and $\mathbf{a}_2$, and the corresponding reciprocal lattice $\mathbf{G}$ has two unit vectors of $\mathbf{b}_1$ and $\mathbf{b}_2$. All crystal layers comprising the multilayer 2D grating along the z-axis direction should have a common primitive lattice and reciprocal lattice.

The EM fields at an arbitrary point $\mathbf{r}$ can be written into the superposition of Bragg waves (or plane waves):

$$\mathbf{E}(\mathbf{r})=\sum_{ij}\mathbf{E}_{ij}(z)e^{i(k_{ij,x}x+k_{ij,y}y)}, \tag{1}$$

$$\mathbf{H}(\mathbf{r})=\sum_{ij}\mathbf{H}_{ij}(z)e^{i(k_{ij,x}x+k_{ij,y}y)}, \tag{2}$$

where the Bragg wave vector $\mathbf{k}_{ij}=(k_{ij,x},k_{ij,y})=(k_{0x},k_{0y})+i\mathbf{b}_1+j\mathbf{b}_2$, $\mathbf{E}_{ij}$ and $\mathbf{H}_{ij}$ are unknown expansion coefficients of the electric and magnetic fields. In principle, the indices i and j should run from $-\infty$ to $+\infty$, but in numerical practice,

[a]Electronic mail: lizy@axel.ameslab.gov

 © 2003 American Institute of Physics

Downloaded 09 Apr 2013 to 171.67.34.205. This article is copyrighted as indicated in the abstract. Reuse of AIP content is subject to the terms at: http://jap.aip.org/about/rights_and_permissions

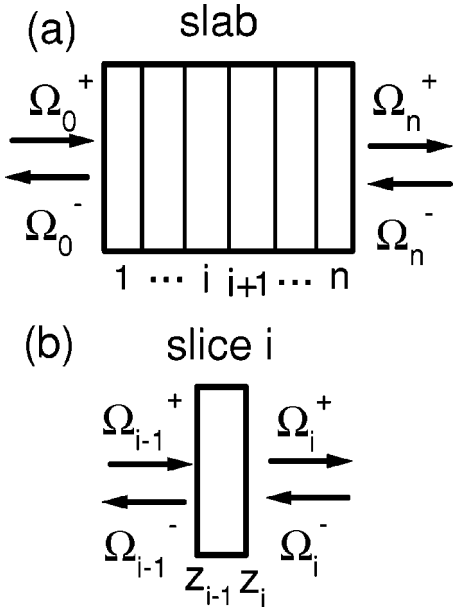

FIG. 1. (a) Definition of the S matrix in the TMM for a photonic crystal slab, which is divided into a number of thin slices; (b) definition of the S matrix for an individual slice.

truncation over a certain order is necessary. To solve the unknown variables $\mathbf{E}_{ij}$ and $\mathbf{H}_{ij}$, the whole photonic crystal slab is divided into a number of thin slices, as shown in Fig. 1(a), where each slice can be approximated as a lamellar 2D grating, within which the dielectric function is constant along the z-axis direction. If the slab has already been a lamellar grating, no division procedure is required. We further imagine that each slice (indexed from 1,2,..., to n) is surrounded by an infinitely thin film of air in the both hand sides. This amounts to placing the whole diffraction problem into a plane wave basis in the air background. These artificial air thin films generate no impact to the diffraction problem, because the thickness of all films is set to zero, and therefore they do not change the continuity of the tangential components of the EM fields at each interface. These tangential fields are the physical variables involved in the TMM, and they are unchanged when these zero-thickness air films are introduced. If the artificial air films have finite thickness, the original physical continuity of fields at each interface is broken because the fields at the two ends of each air film are not identical to each other. The introduction of these air films will bring great numerical flexibility to solve the diffraction problem of our multilayer photonic crystal slabs in a systematic manner.

As shown in Fig. 1(b), the EM fields in the two air thin films around the i_{th} slice consist of forwards and backwards propagating plane waves. The tangential components of the electric field on the left-hand-side air film can be written:

$$E_{x(y)}(\mathbf{r})=\sum_{ij}\left[E^{+}_{ij,x(y)}(z)+E^{-}_{ij,x(y)}(z)\right]e^{ik_{ij,x}x+ik_{ij,y}y}, \quad (3)$$

where $E^{+}_{ij,x(y)}(z)=E^{+}_{ij,x(y)}e^{i\beta_{ij}(z-z_{i-1})}=E^{+}_{ij,x(y)}$, $E^{-}_{ij,x(y)}(z)=E^{-}_{ij,x(y)}e^{-i\beta_{ij}(z-z_{i-1})}=E^{-}_{ij,x(y)}$, since $z=z_{i-1}$. β_{ij} is given by $\beta_{ij}=(k_0^2-k_{ij,x}^2-k_{ij,y}^2)^{1/2}$ for $k_0^2-k_{ij,x}^2-k_{ij,y}^2\geqslant 0$, and $\beta_{ij}=i(k_{ij,x}^2+k_{ij,y}^2-k_0^2)^{1/2}$ for $k_0^2-k_{ij,x}^2-k_{ij,y}^2<0$. The tangential components of the magnetic field are

$$H_{x(y)}(\mathbf{r})=\sum_{ij}\left[H^{+}_{ij,x(y)}(z)+H^{-}_{ij,x(y)}(z)\right]e^{ik_{ij,x}x+ik_{ij,y}y}, \quad (4)$$

where $H^{+}_{ij,x(y)}(z)=H^{+}_{ij,x(y)}$, $H^{-}_{ij,x(y)}(z)=H^{-}_{ij,x(y)}$. For each Bragg wave vector we have the following relation between the $\mathbf{H}$ and $\mathbf{E}$ fields: $(H^{+}_{ij,x},H^{+}_{ij,y})^T=T_{0,ij}(E^{+}_{ij,x},E^{+}_{ij,y})^T$, and $(H^{-}_{ij,x},H^{-}_{ij,y})^T=-T_{0,ij}(E^{-}_{ij,x},E^{-}_{ij,y})^T$, where the superscript "T" denotes matrix transposition. The 2×2 matrix $T_{0,ij}$ has matrix elements $T^{11}_{0,ij}=-k_{ij,x}k_{ij,y}/(k_0\beta_{ij})$, $T^{12}_{0,ij}=(k_{ij,x}^2-k_0^2)/(k_0\beta_{ij})$, $T^{21}_{0,ij}=(k_0^2-k_{ij,y}^2)/(k_0\beta_{ij})$, and $T^{22}_{0,ij}=k_{ix}k_{ij,y}/(k_0\beta_{ij})$. The EM fields on the right-hand-side air film have the same form of expansion. In Eqs. (3) and (4) we simply replace $E^{\pm}_{ij,x(y)}$ and $H^{\pm}_{ij,x(y)}$ with $U^{\pm}_{ij,x(y)}$ and $V^{\pm}_{ij,x(y)}$, respectively. $V^{\pm}_{ij,x(y)}$ and $U^{\pm}_{ij,x(y)}$ also connected each other through the 2×2 matrix $T_{0,ij}$.

Having written the EM fields around the slice, we need to further solve the EM fields inside the 2D lamellar grating slice. This is done by substituting the general plane-wave expansion of fields [Eqs. (1) and (2)] as well as the dielectric function into Maxwell's equations. Finally it will arrive at an eigenproblem whose solutions yield the eigenmodes of EM fields inside the slice. By matching boundary conditions at the two interfaces of the slice, it turns out that the fields at the right-hand side air film are connected to those at the left-hand-side air film by a transfer matrix. For the sake of brevity, we will present the details in Appendix A. The readers can also refer to Refs. 4–9 for more details. By defining column vectors $\Omega^{\pm}_{i-1}=(\ldots,E^{\pm}_{ij,x},E^{\pm}_{ij,y},\ldots)^T$, $\Omega^{\pm}_{i}=(\ldots,U^{\pm}_{ij,x},U^{\pm}_{ij,y},\ldots)^T$, where $-N\leqslant i\leqslant N$, $-M\leqslant j\leqslant M$, with N and M being the truncation orders, we have

$$\begin{pmatrix}\Omega^{+}_{i}\\ \Omega^{-}_{i}\end{pmatrix}=T_i\begin{pmatrix}\Omega^{+}_{i-1}\\ \Omega^{-}_{i-1}\end{pmatrix}=\begin{pmatrix}t^{i}_{11} & t^{i}_{12}\\ t^{i}_{21} & t^{i}_{22}\end{pmatrix}\begin{pmatrix}\Omega^{+}_{i-1}\\ \Omega^{-}_{i-1}\end{pmatrix}. \quad (5)$$

T_i is called the transfer matrix (more accurately, the T matrix) for the i_{th} slice. It is easy to find that the fields in the transmission region $\Omega^{\pm}_{n}$ are connected to the fields in the incident region $\Omega^{\pm}_{0}$ by the total transfer matrix of the slab:

$$\begin{pmatrix}\Omega^{+}_{n}\\ \Omega^{-}_{n}\end{pmatrix}=T\begin{pmatrix}\Omega^{+}_{0}\\ \Omega^{-}_{0}\end{pmatrix}, \quad (6)$$

where $T=T_nT_{n-1}\ldots T_i\ldots T_2T_1$. Notice that $\Omega^{+}_{0}=E_0=(\ldots,0\ldots,E_{0x},E_{0y},\ldots,0,\ldots)^T$, and $\Omega^{-}_{0}=E_r=(\ldots,E^{r}_{ij,x},E^{r}_{ij,y},\ldots)^T$ are column vectors for the incident and reflection waves, $\Omega^{+}_{n}=E_t=(\ldots,E^{t}_{ij,x},E^{t}_{ij,y},\ldots)^T$ is for the transmission waves, while $\Omega^{-}_{n}=0$ since no backwards propagating waves exist in the transmission region. The formula in Eqs. (5) and (6) is called the T-matrix method which is well-known in the grating community. Although simple in nature, this method proves to be numerically unstable for thick gratings such as the photonic crystal slabs studied here. The reason is that the evanescent wave components in the plane-wave expansion will increase exponentially when the T matrices for all slices accumulate, as can be found in Appendix A.

Downloaded 09 Apr 2013 to 171.67.34.205. This article is copyrighted as indicated in the abstract. Reuse of AIP content is subject to the terms at: http://jap.aip.org/about/rights_and_permissions

There are several schemes to overcome this numerical instability. One of them is the scattering-matrix (S-matrix) method.[8] This technique has been adopted in the real-space TMM.[10,11] In this method, the transfer matrix for the i_{th} slice in Eq. (5) is redefined in another way as follows:

$$\begin{pmatrix} \Omega_i^+ \\ \Omega_{i-1}^- \end{pmatrix} = s^i \begin{pmatrix} \Omega_{i-1}^+ \\ \Omega_i^- \end{pmatrix} = \begin{pmatrix} s_{11}^i & s_{12}^i \\ s_{21}^i & s_{22}^i \end{pmatrix} \begin{pmatrix} \Omega_{i-1}^+ \\ \Omega_i^- \end{pmatrix}, \tag{7}$$

where s^i is called the S matrix for slice i. s^i is related with T_i as follows: $s_{11}^i = t_{11}^i - t_{12}^i [t_{22}^i]^{-1} t_{21}^i$, $s_{12}^i = t_{12}^i [t_{22}^i]^{-1}$, $s_{21}^i = -[t_{22}^i]^{-1} t_{21}^i$, $s_{22}^i = [t_{22}^i]^{-1}$. The total S matrix of the whole slab is connected to individual s_i through an iteration algorithm. Suppose the total S matrix for the first $n-1$ slices and the S matrix for slice n have been calculated to be S^{n-1} and s^n, respectively, it can be shown that the total S matrix for the first n slices S^n is given by

$$S_{11}^n = s_{11}^n [I - S_{12}^{n-1} s_{21}^n]^{-1} S_{11}^{n-1}, \tag{8a}$$

$$S_{12}^n = s_{12}^n + s_{11}^n S_{12}^{n-1} [I - s_{21}^n S_{12}^{n-1}]^{-1} s_{22}^{n-1}, \tag{8b}$$

$$S_{21}^n = S_{21}^{n-1} + S_{22}^{n-1} s_{21}^n [I - S_{12}^{n-1} s_{21}^n]^{-1} S_{11}^{n-1}, \tag{8c}$$

$$S_{22}^n = S_{22}^{n-1} [I - s_{21}^n S_{12}^{n-1}]^{-1} s_{22}^n, \tag{8d}$$

where I is a unit matrix, then fields in the transmission and reflection waves are connected to the incident waves through

$$\begin{pmatrix} \Omega_n^+ \\ \Omega_0^- \end{pmatrix} = S^n \begin{pmatrix} \Omega_0^+ \\ \Omega_n^- \end{pmatrix},$$

from which we get

$$E_t = S_{11}^n E_0, \quad E_r = S_{21}^n E_0. \tag{9}$$

After we have obtained coefficients for the reflection and transmission waves, the transmission and reflection spectra are calculated by

$$T = \sum_{ij} T_{ij} = \sum_{ij} \frac{|\mathbf{E}_{ij}^t|^2 |\beta_{ij}|}{|\mathbf{E}_0|^2 |k_{0z}|}, \tag{10}$$

and

$$R = \sum_{ij} R_{ij} = \sum_{ij} \frac{|\mathbf{E}_{ij}^r|^2 |\beta_{ij}|}{|\mathbf{E}_0|^2 |k_{0z}|}, \tag{11}$$

where the summation is run over those homogeneous Bragg waves with lateral wave vectors $k_{ij,x}^2 + k_{ij,y}^2 \leq k_0^2$. $\mathbf{E}_{ij}^t$ and $\mathbf{E}_{ij}^r$ are the amplitudes of the transmission and reflection Bragg wave in the $(ij)_{th}$ order.

In the calculation of the total S matrix for a slab, we can first set $S^0 = I$, which corresponds to the S matrix for an air slice. We then solve the S matrix for slice 1 s^1, and use the iteration algorithm Eqs. (8a)–(8d) to obtain the total S-matrix S^1 for the first one slice. Repeating the procedure, we can finally obtain the total S matrix for the whole slab. Due to the periodicity of the photonic crystal along the z-axis direction, it suffices to only calculate the S-matrix $S(L)$ for a slab one unit cell thick. The S-matrix $S(2L)$ for a slab two unit cells thick is given by

$$S_{11}(2L) = S_{11}(L)[I - S_{12}(L)S_{21}(L)]^{-1} S_{11}(L), \tag{12a}$$

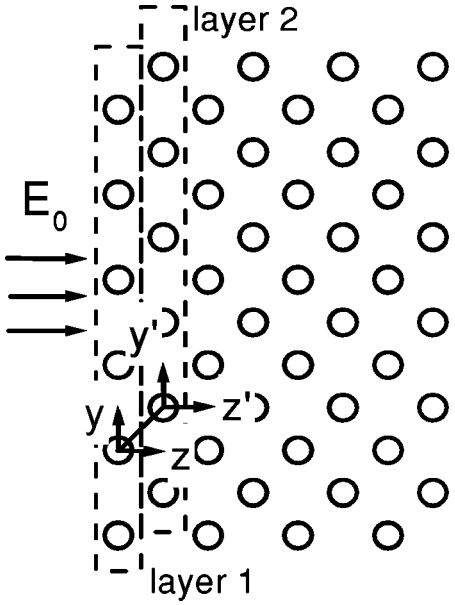

FIG. 2. Schematic of a lattice translational symmetry between two different crystal layers.

$$S_{12}(2L) = S_{12}(L) + S_{11}(L) S_{12}(L)[I - S_{21}(L) S_{12}(L)]^{-1} S_{22}(L), \tag{12b}$$

$$S_{21}(2L) = S_{21}(L) + S_{22}(L) S_{21}(L)[I - S_{12}(L) S_{21}(L)]^{-1} S_{11}(L), \tag{12c}$$

$$S_{22}(2L) = S_{22}(2L)[I - S_{21}(L) S_{12}(L)]^{-1} S_{22}(L). \tag{12d}$$

The S matrix for a photonic crystal slab with arbitrary layers can be calculated in a similar way based on the iteration algorithm Eqs. (8a)–(8d).

III. LATTICE SYMMETRY APPLIED IN THE TRANSFER-MATRIX METHOD

In Sec. II we find that the transfer matrix $S(L)$ for a slab one unit cell thick plays a key role in the solution of wave diffraction problem due to the periodicity of the photonic crystal. However, another characteristic of a photonic crystal, the intrinsic lattice symmetry, has so far not been considered in previous studies of the TMM. In the following, it will become clear that these intrinsic lattice symmetries in a photonic crystal, if fully exploited, can greatly simplify the solution of the TMM.

For the sake of clarity to our discussion, let us first look at an example. Consider a 2D photonic crystal slab whose schematic configuration is shown in Fig. 2. The crystal consists of a square lattice of infinitely long dielectric cylinders in air, with one layer stacked with another along the (11) direction of the crystal. In this 1D grating, the lattice spacing is $\sqrt{2}\,a$, where a is the lattice constant of a square lattice. The unit cell repeats itself every two layers of cylinders along the stacking direction, with the second layer translated laterally with respect to the first layer by $\sqrt{2}/2\,a$. If the photonic crystal slab has a stacking direction along other planes, such as the (12) and (13) planes, a unit cell would consist of more layers of cylinders.

Downloaded 09 Apr 2013 to 171.67.34.205. This article is copyrighted as indicated in the abstract. Reuse of AIP content is subject to the terms at: http://jap.aip.org/about/rights_and_permissions

In this photonic crystal slab, we face a translational symmetry. One easily notices that the second layer of cylinders in Fig. 2 is identical in structure to the first layer, except for a lateral translation of $\sqrt{2}/2\,a$. It turns out that there is simple relation between the transfer matrices for these two layers, which we show can be analytically evaluated. Therefore, instead of the need to solve the transfer matrix numerically for a slab consisting two or more layers of cylinders by following the procedures developed in Sec. II slice by slice from the first layer to the final within one unit cell, only the transfer matrix for a single layer of cylinders is now required. This surely will reduce the numerical effort significantly.

To see how a translational symmetry can be applied to the TMM, for generality, we still consider a 2D grating made up of a 3D photonic crystal slab, and confine ourselves to the S-matrix formalism. Suppose we have numerically solved the transfer matrix S_1 for the first layer, then suppose that the second layer is obtained by the following translational transformation of coordinates from the first layer:

$$x \rightarrow x' + x_0, \;\; y \rightarrow y' + y_0, \tag{13}$$

where (x,y) and (x',y') are original and new coordinates, and (x_0,y_0) are relative translations between the two frames. Obviously in the frame of the new coordinates (x',y'), the second layer has the same transfer matrix of $S'=S_1$. Let us write Eq. (7) in a more detailed form where the two tangential field components become explicit:

$$\begin{pmatrix} \Omega'^{+}_{1x}(k'_{i,j}) \\ \Omega'^{+}_{1y}(k'_{i,j}) \\ \Omega'^{-}_{0x}(k'_{i,j}) \\ \Omega'^{-}_{0y}(k'_{i,j}) \end{pmatrix} = \begin{pmatrix} S'^{(11)}_{11} & S'^{(12)}_{11} & S^{(11)}_{12} & S'^{(12)}_{12} \\ S'^{(21)}_{11} & S'^{(22)}_{11} & S'^{(21)}_{12} & S'^{(22)}_{12} \\ S'^{(11)}_{21} & S'^{(12)}_{21} & S'^{(11)}_{22} & S'^{(12)}_{12} \\ S'^{(21)}_{21} & S'^{(22)}_{21} & S'^{(21)}_{22} & S'^{(22)}_{12} \end{pmatrix} \times \begin{pmatrix} \Omega'^{+}_{0x}(k'_{m,n}) \\ \Omega'^{+}_{0y}(k'_{m,n}) \\ \Omega'^{-}_{1x}(k'_{m,n}) \\ \Omega'^{-}_{1y}(k'_{m,n}) \end{pmatrix}. \tag{14}$$

The subscripts ij $(i,j=1,2)$ denote four block submatrices of the S matrix, while the superscripts ij $(i,j=1,2)$ are for the x and y components of the electric field. $S'^{(11)}_{11} = S'^{(11)}_{11}(i,j;m,n)$, etc. are matrix elements of the S matrix in which the indices i, j, m, and n have been neglected. With this S matrix at hand, we need to turn back to the corresponding S matrix in the original coordinates, which is recorded as S and satisfies

$$\begin{pmatrix} \Omega^{+}_{1x}(k_{i,j}) \\ \Omega^{+}_{1y}(k_{i,j}) \\ \Omega^{-}_{0x}(k_{i,j}) \\ \Omega^{-}_{0y}(k_{i,j}) \end{pmatrix} = \begin{pmatrix} S^{(11)}_{11} & S^{(12)}_{11} & S^{(11)}_{12} & S^{(12)}_{12} \\ S^{(21)}_{11} & S^{(22)}_{11} & S^{(21)}_{12} & S^{(22)}_{12} \\ S^{(11)}_{21} & S^{(12)}_{21} & S^{(11)}_{22} & S^{(12)}_{12} \\ S^{(21)}_{21} & S^{(22)}_{21} & S^{(21)}_{22} & S^{(22)}_{12} \end{pmatrix} \times \begin{pmatrix} \Omega^{+}_{0x}(k_{m,n}) \\ \Omega^{+}_{0y}(k_{m,n}) \\ \Omega^{-}_{1x}(k_{m,n}) \\ \Omega^{-}_{1y}(k_{m,n}) \end{pmatrix}. \tag{15}$$

Under the axis translation Eq. (13), the amplitudes of the field vectors (including the directions) and wave vectors (including the reciprocal lattice vectors $\mathbf{G}$ and the incident wave vector $\mathbf{k}_0$) keep unchanged:

$$(k_x,k_y) \rightarrow (k'_x,k'_y), \;\; (E_x,E_y) \rightarrow (E'_x,E'_y), \tag{16}$$

so, each plane-wave component of the EM fields is transformed according to

$$\begin{aligned} & E_{x(y)}(k_{i,j}) e^{ik_{ij,x}x + ik_{ij,y}} \\ & \quad \rightarrow E'_{x(y)}(k'_{i,j}) e^{ik'_{ij,x}x' + ik'_{ij,y}y'} \\ & \quad = E'_{x(y)}(k'_{i,j}) e^{ik_{ij,x}x + ik_{ij,y}y} e^{ik_{ij,x}x_0 + ik_{ij,y}y_0}. \end{aligned}$$

This leads to the following transformation:

$$E_{x(y)}(k_{i,j}) \rightarrow E'_{x(y)}(k'_{i,j}) e^{ik_{ij,x}x_0 + ik_{ij,y}y_0}. \tag{17}$$

Substituting Eq. (17) into Eq. (15) yields

$$\begin{aligned} & \begin{pmatrix} \Omega'^{+}_{1x}(k'_{i,j}) e^{ik_{ij,x}x_0 + ik_{ij,y}y_0} \\ \Omega'^{+}_{1y}(k_{i,j}) e^{ik_{ij,x}x_0 + ik_{ij,y}y_0} \\ \Omega'^{-}_{0x}(k_{i,j}) e^{ik_{ij,x}x_0 + ik_{ij,y}y_0} \\ \Omega'^{-}_{0y}(k_{i,j}) e^{ik_{ij,x}x_0 + ik_{ij,y}y_0} \end{pmatrix} \\ & \quad = \begin{pmatrix} S^{(11)}_{11} & S^{(12)}_{11} & S^{(11)}_{12} & S^{(12)}_{12} \\ S^{(21)}_{11} & S^{(22)}_{11} & S^{(21)}_{12} & S^{(22)}_{12} \\ S^{(11)}_{21} & S^{(12)}_{21} & S^{(11)}_{22} & S^{(12)}_{12} \\ S^{(21)}_{21} & S^{(22)}_{21} & S^{(21)}_{22} & S^{(22)}_{12} \end{pmatrix} \\ & \qquad \times \begin{pmatrix} \Omega'^{+}_{0x}(k_{m,n}) e^{ik_{mn,x}x_0 + ik_{mn,y}y_0} \\ \Omega'^{+}_{0y}(k_{m,n}) e^{ik_{mn,x}x_0 + ik_{mn,y}y_0} \\ \Omega'^{-}_{1x}(k_{m,n}) e^{ik_{mn,x}x_0 + ik_{mn,y}y_0} \\ \Omega'^{-}_{1y}(k_{m,n}) e^{ik_{mn,x}x_0 + ik_{mn,y}y_0} \end{pmatrix}. \end{aligned} \tag{18}$$

Comparing Eq. (18) with Eq. (14), we find the following transformation of the S matrix under the axis translation,

$$\begin{aligned} & S'^{(11)}_{11}(i,j;m,n) e^{i(k_{ij,x} - k_{mn,x})x_0 + i(k_{ij,y} - k_{mn,y})y_0} \\ & \quad \rightarrow S^{(11)}_{11}(i,j;m,n). \end{aligned} \tag{19}$$

Other matrix elements $S'^{(mn)}_{ij}$ and $S^{(mn)}_{ij}$ $(i,j,m,n=1,2)$ are subject to the same transformation rule.

A lattice translational symmetry is quite general in a photonic crystal slab with an arbitrary stacking direction of crystal layers. The transformation rule derived in Eq. (19) is universally applicable to any lattice type and any configuration of the building block of the crystal. In a 2D photonic crystal slab, such as the structure shown in Fig. 2, this is the only available lattice symmetry. For a 3D photonic crystal slab, there is another type of lattice symmetry operation, a coordinate rotation. However, basic crystallography requests that a layer after rotation still be in the same lattice as the original one. In addition, the Bragg wave vectors should stay in the same group before and after the coordinate rotation. This will impose strong limitation to the relative rotation angle between two crystal layers as well as the incident angle of external waves. In the following, we will take a simple example to see how a transfer matrix is transformed under a coordinate rotation.

Downloaded 09 Apr 2013 to 171.67.34.205. This article is copyrighted as indicated in the abstract. Reuse of AIP content is subject to the terms at: http://jap.aip.org/about/rights_and_permissions

Consider a plane EM wave normally incident on a 2D grating arrayed in a square lattice in the lateral plane. Suppose the first crystal layer is identical to the second layer after a 90° rotation of coordinate. We can see that all the above limits are satisfied here. The coordinates are transformed according to

$$y \rightarrow x', \quad x \rightarrow -y', \tag{20}$$

where x, y and x', y' are coordinates in the original and the new rotated frames. Both Bragg wave vectors and the amplitudes of the EM field vectors should be transformed in the same way:

$$(k_x, k_y) \rightarrow (-k'_y, k'_x), \quad (E_x, E_y) \rightarrow (-E'_y, E'_x). \tag{21}$$

Suppose that S' and S are the S matrix in the rotated and original coordinates, respectively. They satisfy

$$\begin{pmatrix} \Omega'^{+}_{1x}(k'_{i,j}) \\ \Omega'^{+}_{1y}(k'_{i,j}) \\ \Omega'^{-}_{0x}(k'_{i,j}) \\ \Omega'^{-}_{0y}(k'_{i,j}) \end{pmatrix} = \begin{pmatrix} S'^{(11)}_{11} & S'^{(12)}_{11} & S'^{(11)}_{12} & S'^{(12)}_{12} \\ S'^{(21)}_{11} & S'^{(22)}_{11} & S'^{(21)}_{12} & S'^{(22)}_{12} \\ S'^{(11)}_{21} & S'^{(12)}_{21} & S'^{(11)}_{22} & S'^{(12)}_{12} \\ S'^{(21)}_{21} & S'^{(22)}_{21} & S'^{(21)}_{22} & S'^{(22)}_{12} \end{pmatrix} \times \begin{pmatrix} \Omega'^{+}_{0x}(k'_{m,n}) \\ \Omega'^{+}_{0y}(k'_{m,n}) \\ \Omega'^{-}_{1x}(k'_{m,n}) \\ \Omega'^{-}_{1y}(k'_{m,n}) \end{pmatrix}, \tag{22}$$

and

$$\begin{pmatrix} \Omega^{+}_{1x}(k_{i,j}) \\ \Omega^{+}_{1y}(k_{i,j}) \\ \Omega^{-}_{0x}(k_{i,j}) \\ \Omega^{-}_{0y}(k_{i,j}) \end{pmatrix} = \begin{pmatrix} S^{(11)}_{11} & S^{(12)}_{11} & S^{(11)}_{12} & S^{(12)}_{12} \\ S^{(21)}_{11} & S^{(22)}_{11} & S^{(21)}_{12} & S^{(22)}_{12} \\ S^{(11)}_{21} & S^{(12)}_{21} & S^{(11)}_{22} & S^{(12)}_{12} \\ S^{(21)}_{21} & S^{(22)}_{21} & S^{(21)}_{22} & S^{(22)}_{12} \end{pmatrix} \times \begin{pmatrix} \Omega^{+}_{0x}(k_{m,n}) \\ \Omega^{+}_{0y}(k_{m,n}) \\ \Omega^{-}_{1x}(k_{m,n}) \\ \Omega^{-}_{1y}(k_{m,n}) \end{pmatrix}. \tag{23}$$

The matrix S' is supposed to be known from the calculation of the first layer, $S' = S_1$. Transforming Eq. (23) into the rotated coordinates leads to

$$\begin{pmatrix} -\Omega'^{+}_{1y}(k'_{-j,i}) \\ \Omega'^{+}_{1x}(k'_{-j,i}) \\ -\Omega'^{-}_{0y}(k'_{-j,i}) \\ \Omega'^{-}_{0x}(k'_{-j,i}) \end{pmatrix} = \begin{pmatrix} S^{(11)}_{11} & S^{(12)}_{11} & S^{(11)}_{12} & S^{(12)}_{12} \\ S^{(21)}_{11} & S^{(22)}_{11} & S^{(21)}_{12} & S^{(22)}_{12} \\ S^{(11)}_{21} & S^{(12)}_{21} & S^{(11)}_{22} & S^{(12)}_{12} \\ S^{(21)}_{21} & S^{(22)}_{21} & S^{(21)}_{22} & S^{(22)}_{12} \end{pmatrix} \times \begin{pmatrix} -\Omega'^{+}_{0y}(k'_{-n,m}) \\ \Omega'^{+}_{0x}(k'_{-n,m}) \\ -\Omega'^{-}_{1y}(k'_{-n,m}) \\ \Omega'^{-}_{1x}(k'_{-n,m}) \end{pmatrix}. \tag{24}$$

Comparing Eq. (24) with Eq. (22), we obtain the transformation of an S matrix under a 90° axis rotation:

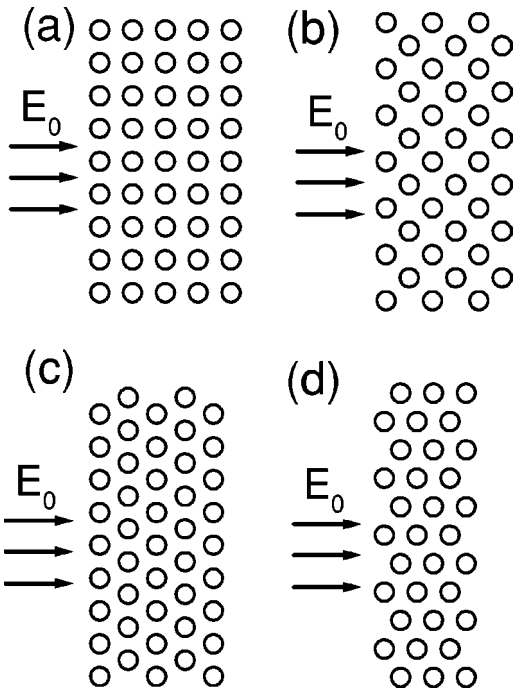

FIG. 3. Schematic of a 2D photonic crystal slab made up of infinitely long dielectric cylinders in air. In (a) and (b) the layers of cylinders are stacked along the (10) and (11) direction of a square lattice, respectively. In (c) and (d) the layers are stacked along a direction perpendicular and parallel to one side of a hexagon in a triangular lattice, respectively.

$$\begin{aligned} &S'^{(22)}_{11}(-j,i;-n,m) \rightarrow S^{(11)}_{11}(i,j;m,n), \\ &-S'^{(21)}_{11}(-j,i;-n,m) \rightarrow S^{(12)}_{11}(i,j;m,n), \\ &-S'^{(12)}_{11}(-j,i;-n,m) \rightarrow S^{(21)}_{11}(i,j;m,n), \\ &S'^{(11)}_{11}(-j,i;-n,m) \rightarrow S^{(22)}_{11}(i,j;m,n). \end{aligned} \tag{25}$$

The same transformation rule applies to other block submatrices S_{12}, S_{21}, and S_{22}.

In the above we only consider lattice symmetries applied to the S-matrix formalism. However, a close look at the general TMM indicates that the same transformation rules derived above are also applicable to other formalisms, such as the T-matrix formalism [see Eq. (5)] and R-matrix formalism.[8,9] This is because the transfer matrix in all formalisms have the same configuration with respect to the Bragg wave vectors and tangential field components, and these are the only quantities subject to coordinate transformations.

IV. RESULTS AND DISCUSSIONS

Now that we have settled the formalism for the lattice translational and rotational symmetries applied in the TMM, we move forward to consider some examples to demonstrate the power of this method in treating wave propagation through a photonic crystal slab. First we consider a 2D photonic crystal slab consisting of a square lattice of dielectric cylinders in air as shown in Fig. 3(a). The crystal layers are stacked along the (10) direction, and a single layer of cylinders comprises a repeating unit cell along the z-axis direction. A more complex configuration is shown in Fig. 3(b),

Downloaded 09 Apr 2013 to 171.67.34.205. This article is copyrighted as indicated in the abstract. Reuse of AIP content is subject to the terms at: http://jap.aip.org/about/rights_and_permissions

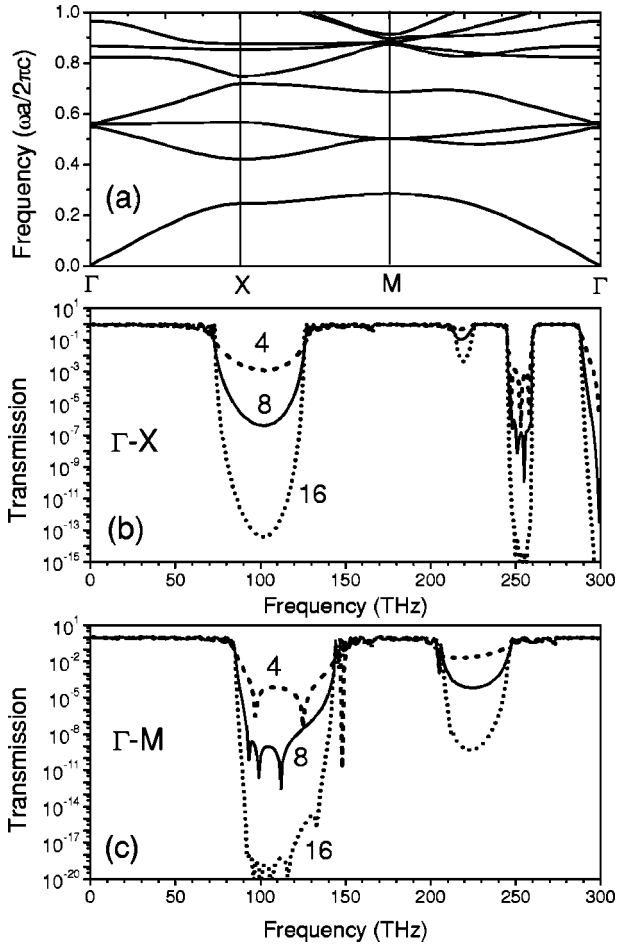

FIG. 4. (a) Photonic band structure plots of the E-polarization mode for a square lattice of dielectric cylinders in air, where the lattice constant is $a=1\ \mu$m, the radius of cylinders is $r=0.2a$, and the refractive index of cylinders is $n=3.4$; (b) and (c) are transmission spectra for an E-polarized plane wave normally incident on the slab as shown in Figs. 3(a) and 3(b) corresponding to the $\Gamma-X$ and $\Gamma-M$ direction in (a), respectively. Three samples consisting of 4, 8, and 16 layers of cylinders are considered.

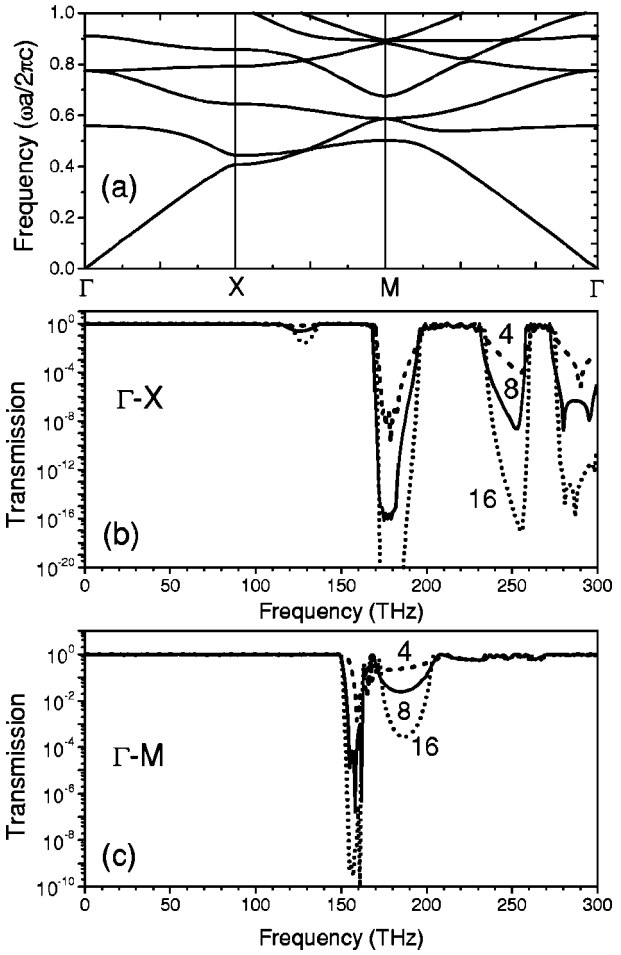

FIG. 5. Same as in Fig. 4, except for the H-polarization mode.

where the layers are stacked along the (11) direction of the crystal. Two layers of cylinders build up a repeating unit cell, and the second layer in each unit cell is translated laterally by $\sqrt{2}/2\,a$ from the first layer. In this structure, it suffices to only calculate the S-matrix S_1 for the first layer, whereas the S matrix for the second layer S_2 can be analytically derived by a translational transformation on S_1 following Eq. (19). Then the S-matrix $S(L)$ for a repeating unit cell is obtained by the iteration algorithm Eqs. 8(a)–8(d) on S_1 and S_2. We have considered a crystal with a lattice spacing $a=1\ \mu$m, a radius of cylinder $r=0.2a$, and a refractive index of cylinder $n=3.4$. The calculated transmission spectrum for an E-polarized (with the electric field parallel to the cylinder axis) plane wave normally incident on the slab is displayed in Figs. 4(b) and 4(c) for the slabs shown in Figs. 3(a) and 3(b), respectively. In both slabs, samples consisting of 4, 8, and 16 layers of cylinders are considered. 21 plane waves are used in the calculations, and good convergence is achieved. To have a reference of our numerical calculations, we calculate the photonic band structures for this photonic crystal using the plane-wave expansion method,[12–15] and the results are displayed in Fig. 4(a) along the high-symmetry lines of the first Brillouin zone. In our calculations, we use 625 plane waves. Note the $\Gamma-X$ and $\Gamma-M$ lines correspond to the surface normal of the two slabs in Figs. 3(a) and 3(b), respectively. Therefore, the directional band gap appearing in the band structure should also be visible from the transmission spectra. This is exactly the case. There is a wide band gap in the lower bands along both the $\Gamma-X$ and $\Gamma-M$ directions, lying between a normalized frequency 0.246 and 0.421 $(2\pi c/a)$ and 0.286 and 0.479 $(2\pi c/a)$, respectively, where c is the light speed in vacuum. With $a=1\ \mu$m, the band gap lies between 73.8 and 126.3 and 85.8 and 143.7 THz, respectively. In Fig. 4(b), the transmittance is below 1% between 74 and 125 THz for the eight-layer sample, while in Fig. 4(c), the transmittance between 86 and 143 THz is below 1% for the eight-layer sample. The agreement between photonic band structures and tranmission spectra calculations is good, indicating the correctness and efficiency of the proposed lattice-symmetry enhanced TMM. The agreement between the two calculations on higher directional band gaps is also quite promising.

We also consider an H-polarized (with the magnetic field parallel to the cylinder axis) plane wave normally incident on the two photonic crystal slabs. The calculated photonic band structures and transmission spectra for the two slabs are displayed in Figs. 5(a), 5(b), and 5(c), respectively. As can be

Downloaded 09 Apr 2013 to 171.67.34.205. This article is copyrighted as indicated in the abstract. Reuse of AIP content is subject to the terms at: http://jap.aip.org/about/rights_and_permissions

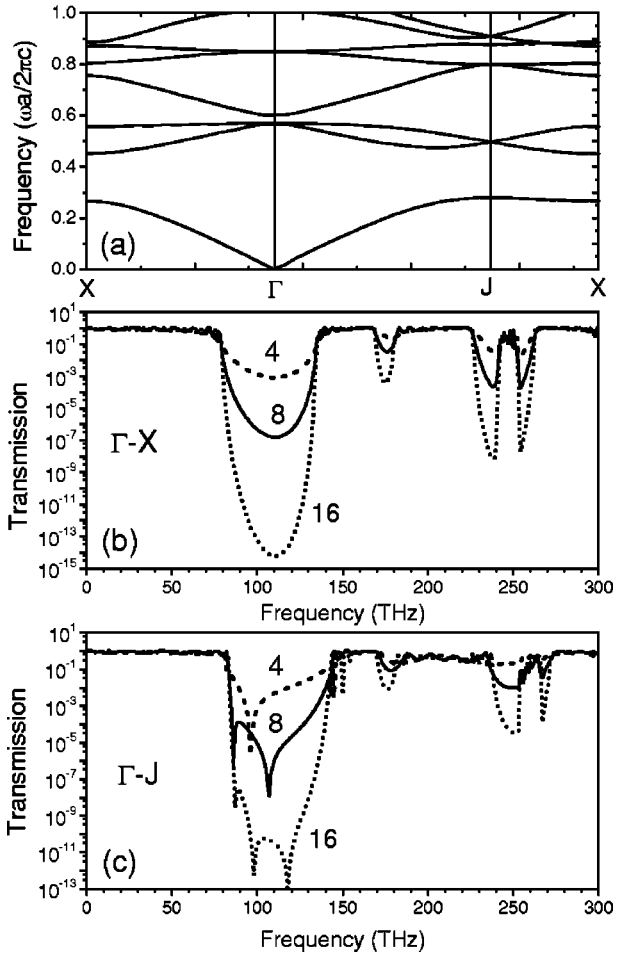

FIG. 6. (a) Photonic band structure plots of the E-polarization mode for a triangular lattice of dielectric cylinders in air, where $a=1\ \mu$m, $r=0.2a$, and $n=3.4$; (b) and (c) are transmission spectra for an E-polarized plane wave normally incident on the slab as shown in Figs. 3(c) and 3(d) corresponding to the $\Gamma-X$ and $\Gamma-J$ direction in (a), respectively. Three samples consisting of 4, 8, and 16 layers of cylinders are considered.

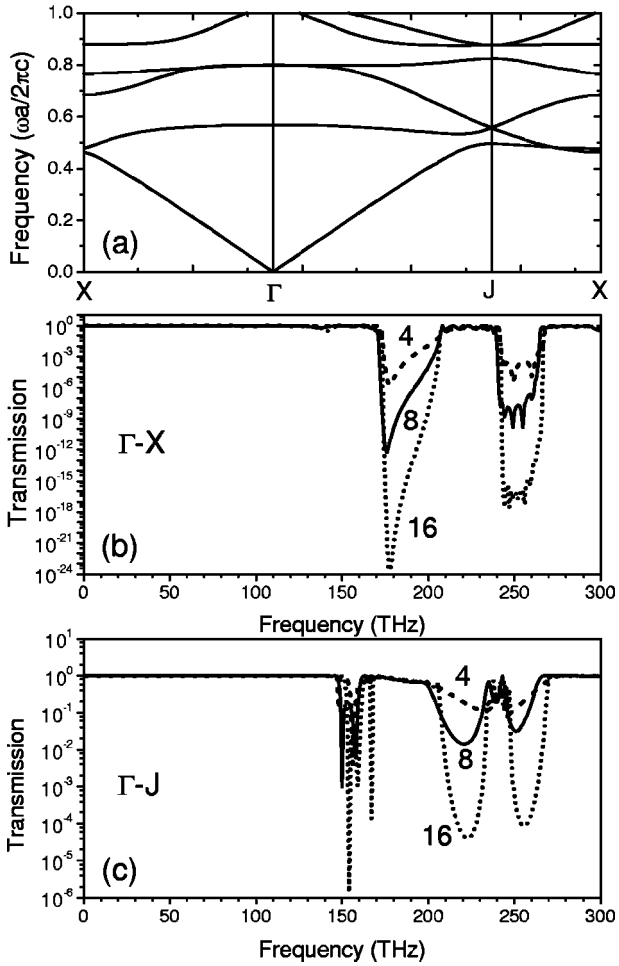

FIG. 7. Same as in Fig. 6, except for the H-polarization mode.

found in Fig. 5(a), there are three directional band gaps along the $\Gamma-X$ direction [(10) direction], lying between 0.407 and 0.444, 0.561 and 0.646, and 0.792 and 0.857 $(2\pi c/a)$, corresponding to 122–133, 168–194, and 238–257 THz, respectively. The results are in agreement with the transmission spectra shown in Fig. 5(b). There is only one narrow band gap along the $\Gamma-M$ direction [(11) direction], lying at 0.501–0.540 $(2\pi c/a)$, corresponding to 150–162 THz, also in agreement with the tranmission spectrum displayed in Fig. 5(c). A transmission dip appears between 170 and 200 THz along the (11) direction. The transmittance keeps decaying when the layer number is increased. This seems to indicate the presence of a band gap. However, we do not find the corresponding band gap in Fig. 5(a) and the dip is far shallower than the real band gap at lower frequency. It might be a pseudo-gap induced by poor coupling of the incident wave with the Bloch's modes at the third photonic band along the $\Gamma-M$ direction.

Another photonic crystal structure, a triangular lattice of dielectric cylinders in air, turns out slightly more complex than the square lattice. As the two primitive lattice vectors $\mathbf{a}_1$ and $\mathbf{a}_2$ are not orthogonal to each other, the lattice symmetry can find its place of application in any photonic crystal slab. In our example, we still consider a structure with $a=1\ \mu$m, $r=0.2a$, and $n=3.4$. The corresponding photonic band structures are plotted in Figs. 6(a) and 7(a) for the E and H polarization modes, respectively. Corresponding to the two high-symmetry lines $\Gamma-X$ and $\Gamma-J$, the photonic crystal slab should be stacked in a way schematically shown in Figs. 3(c) and 3(d), respectively. In both slabs each repeating unit cell of the 1D grating is composed of two layers of cylinders. The calculated transmission spectra for the two slabs are plotted in Figs. 6(b) and 6(c), respectively, for normal incidence of E-polarized plane wave, while the spectra for the H polarization are displayed in Figs. 7(b) and 7(c). Three samples consisting of 4, 8, and 16 layers of cylinders are also considered. Good agreement is also found between the band structures and transmission spectra calculations in regard to the band-gap position. For example, according to Fig. 6(a), a wide E-polarization band gap opens between 0.266 and 0.450 and 0.279 and 0.475 $(2\pi c/a)$ along the $\Gamma-X$ and $\Gamma-J$ directions, corresponding to a frequency of 79.8–135 and 83.7–142.5 THz, respectively. In Figs. 6(b) and 6(c), the lowest transmission dip lies between 80 and 133 and 84 and 143 THz, respectively, within which the maximum transmittance is below 1% for the eight-layer sample.

Downloaded 09 Apr 2013 to 171.67.34.205. This article is copyrighted as indicated in the abstract. Reuse of AIP content is subject to the terms at: http://jap.aip.org/about/rights_and_permissions

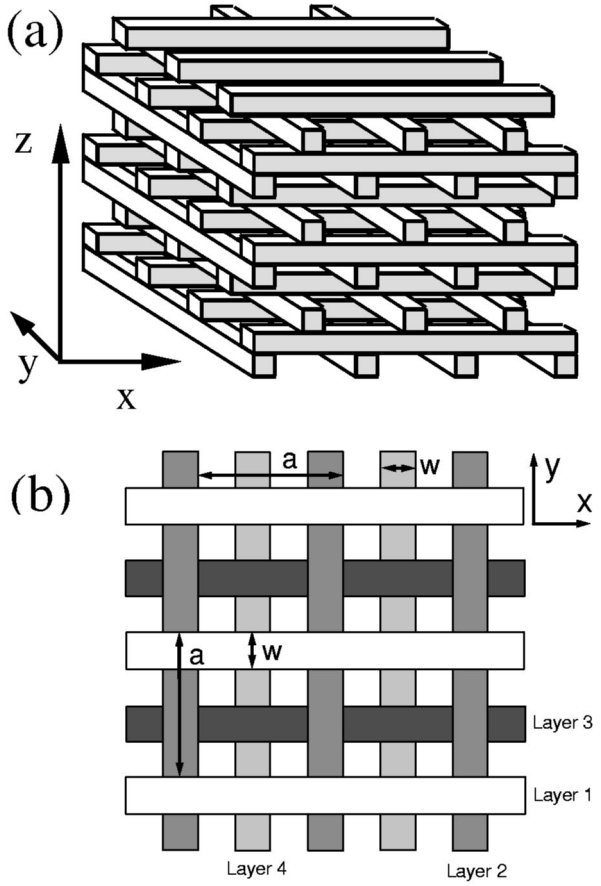

FIG. 8. (a) Schematic configuration of a 3D layer-by-layer photonic crystal composed of rectangular dielectric rods in air; (b) top-view image of (a) from the (001) direction, the stacking direction of the crystal layers.

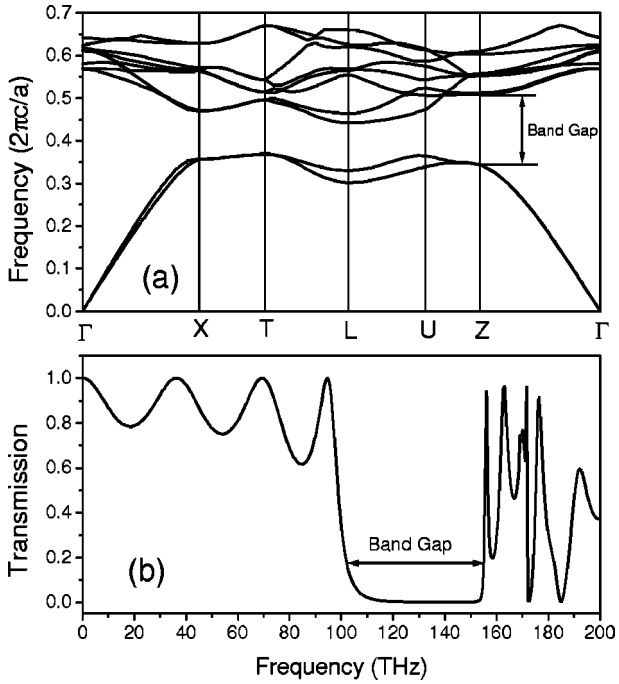

FIG. 9. (a) Plots of photonic band structures along some high-symmetry lines of the first Brillouin zone of the fct lattice. The crystal is of a rod-to-rod spacing 1 μm, a rod width and thickness 0.25 and 0.3125 μm, respectively, and a refractive index of the rods $n=3.4$; (b) transmission spectrum for a plane wave normally incident on an eight-layer photonic crystal slab along the (001) direction, corresponding to the $\Gamma-Z$ direction in (a). The wave is polarized so that the electric field is parallel to the rods in the first layer.

Now we turn to a 3D photonic crystal slab, where the translational

and rotational symmetries might be existing at the same time. Consider a well-known 3D layer-by-layer photonic crystal[16,17] as schematically shown in Fig. 8(a), whose corresponding top-view picture along the (001) direction is shown in Fig. 8(b). The photonic crystal is formed by stacking rectangular dielectric rods layer by layer consecutively along the (001) direction. Rods in each layer are arrayed into a 1D lamellar grating with a pitch of a. Rods in one layer are perpendicular to those in the next layer, while rods in one layer are shifted by $a/2$ with respect to those in the next two layers. The primitive unit cell of the photonic crystal is arrayed into a face-centered tetragonal (fct) lattice. In Figs. 8(a) and 8(b), we have assumed that rods in the first layer are along the x axis, and rods in the second layer are along the y-axis direction, etc. Each of the rods has a width of w, a thickness of h, and form a square lattice with a lattice spacing of a in the (001) plane. Four layers of rods comprise a repeating unit cell along the (001) direction of the crystal.

In the conventional TMM, one needs to calculate the transfer matrix for a slab composed of a repeating unit cell, namely, four layers as a whole. However, a close look at the 2D grating structure shows that there are beautiful translational and rotational symmetries among different layers. The second layer, with rods directed along the y axis, is a 90° rotation from the first layer. The third layer is translated by $a/2$ from the first layer along the y axis, and the fourth layer is translated from the second layer by $a/2$ along the x axis. In other words, the third and fourth layers as a whole are translated from the first and second layers by $(a/2,a/2)$. Therefore, in the situation of normal incidence of a plane wave, we can calculate the transfer matrix for the whole unit cell as follows. We first calculate the S matrix for the first layer S_1. Performing a 90° rotational transformation according to Eq. (25) on S_1 will yield the S-matrix S_2 for the second layer. The S-matrix S_{12} for the first two layers can be calculated from S_1 and S_2 using iteration formula Eqs. 8(a)–8(d). Then the S-matrix S_{34} for the third and fourth layers as a whole can be obtained by performing a translational transformation over S_{12}. After a combination of S_{12} and S_{34} using the iteration formula, the S-matrix $S(L)$ for the unit cell is readily calculated. In this way, a photonic crystal slab consisting of any number of layers can be calculated iteratively.

Figure 9(a) displays the calculated photonic band structures along some high-symmetry lines of the first Brillouin zone of the fct lattice. 721 plane waves are used to expand the EM fields. The photonic crystal is of parameters of $a=1$ μm, $w=0.25a$, and $h=0.3125a$. The refractive index of the rods is $n=3.4$. In Fig. 9(a), $\Gamma-X$ and $\Gamma-Z$ correspond to the (100) and (001) direction of the lattice. There is a wide band gap along the (001) direction lying between a normalized frequency 0.349–0.508 $(2\pi c/a)$. With $a=1$ μm, the band gap is at 104.7–152.4 THz. Figure 9(b) is the calculated transmission spectrum for a normally incident

Downloaded 09 Apr 2013 to 171.67.34.205. This article is copyrighted as indicated in the abstract. Reuse of AIP content is subject to the terms at: http://jap.aip.org/about/rights_and_permissions

x-polarized plane wave propagating through an eight-layer (2 unit-cell thick) photonic crystal slab. 9×9 plane waves are used in the TMM calculations. A transmission dip is located between 104 and 153 THz, within which the minimum transmittance is about 10^{-4}. The result of the band-gap position agrees quite well with the band structure calculation. In other directions, some lattice symmetries still exist that can be utilized to simplify the transfer-matrix calculation. The use of lattice symmetry not only reduces the computational burden, but also improves the efficiency of the TMM, due to the incorporation of a large amount of analytical manipulations.

In the above discussion, we only consider lattice symmetries (including universal translational symmetry and special rotational symmetry) among different layers of a photonic crystal to reduce numerical simulation involved in the TMM. Structural symmetry within a single layer can also remarkably reduce the numerical burden of TMM simulations. We take the scattering problem of Fig. 2 as an example. There is a mirror-reflection symmetry with respect to the y axis in the case of normal incidence. Then in the plane-wave based TMM, the coefficient of the $+k_y$ wave component has a definite symmetric relation with the coefficient of the $-k_y$ wave component. This means that we need to only consider those $+k_y$ wave components in the TMM, and as a result the matrix size has been reduced to one half, which can significantly relieve the numerical burden. Unlike the universal translational symmetry discussed above, the mirror-reflection symmetry only holds in the special normal-incidence situation. This will impose a strong limitation to its application.

V. SUMMARY AND CONCLUSION

In summary, we have developed a formalism of the TMM to investigate EM waves propagation through a photonic crystal slab. The intrinsic lattice symmetry such as the translational and rotational symmetries between different crystal layers can be utilized to significantly reduce the numerical computation of transfer matrices for these layers by means of analytical matrix transformations. The results of transmission and reflection spectra obtained by this lattice symmetry enhanced TMM for 2D and 3D photonic crystal slabs are all in good agreement with the photonic band structure calculations in predicting the position of a photonic band gap. This indicates that the proposed method is accurate and efficient in handling wave diffraction problems of photonic crystals.

ACKNOWLEDGMENT

Ames Laboratory is operated for the U.S. Department of Energy (DOE) by Iowa State University under Contract No. W-7405-ENG-82.

APPENDIX A: EIGENMODES WITHIN A 2D LAMELLAR GRATING SLICE AND THE RESULTING TRANSFER MATRIX

In this appendix we will present a detailed description on how the eigenmode of EM fields within a 2D lamellar grating slice is solved, and how the transfer matrix connecting fields at the two hand sides of this grating slice is related to these eigenmodes.

We start from Maxwell's equations:

$$\nabla\times\mathbf{E}(\mathbf{r})=ik_0\mathbf{H}(\mathbf{r}),\quad \nabla\times\mathbf{H}(\mathbf{r})=-ik_0\epsilon(\mathbf{r})\mathbf{E}(\mathbf{r}). \tag{A1}$$

Here $\epsilon(\mathbf{r})$ is the periodic dielectric function of the grating slice, it is homogeneous along the z-axis direction. We can rewrite Eq. (A1) into six partial-differential equations satisfied by (E_x,E_y,E_z) and (H_x,H_y,H_z). The z components of EM fields E_z and H_z can be deleted from these six equations, leading to the following four coupled equations:

$$\frac{\partial}{\partial z}E_x=\frac{1}{-ik_0}\frac{\partial}{\partial x}\left[\frac{1}{\epsilon}\left(\frac{\partial}{\partial x}H_y-\frac{\partial}{\partial y}H_x\right)\right]+ik_0H_y, \tag{A2}$$

$$\frac{\partial}{\partial z}E_y=\frac{1}{-ik_0}\frac{\partial}{\partial y}\left[\frac{1}{\epsilon}\left(\frac{\partial}{\partial x}H_y-\frac{\partial}{\partial y}H_x\right)\right]-ik_0H_x, \tag{A3}$$

$$\frac{\partial}{\partial z}H_x=\frac{1}{ik_0}\frac{\partial}{\partial x}\left(\frac{\partial}{\partial x}E_y-\frac{\partial}{\partial y}E_x\right)-ik_0\epsilon E_y, \tag{A4}$$

$$\frac{\partial}{\partial z}H_y=\frac{1}{ik_0}\frac{\partial}{\partial y}\left(\frac{\partial}{\partial x}E_y-\frac{\partial}{\partial y}E_x\right)+ik_0\epsilon E_x. \tag{A5}$$

We can further write the plane-wave expansion expressions of the EM fields [already given in Eqs. (1) and (2)] and the dielectric function

$$\epsilon(\mathbf{r})=\sum_{ij}\ \epsilon_{i,j}e^{i\mathbf{G}_{ij}\cdot\mathbf{r}}, \tag{A6}$$

$$\epsilon^{-1}(\mathbf{r})=\sum_{ij}\ \epsilon_{i,j}^{-1}e^{i\mathbf{G}_{ij}\cdot\mathbf{r}}. \tag{A7}$$

The expansion in Eqs. (A6) and (A7) is only formal. In our practice of numerical simulations, we have fully considered the advanced Fourier expansion rules developed in literature for both the 2D and 3D periodic structures (see, for instance, Refs. 7 and 8 for details) for these two functions in order to achieve optimal numerical convergency.

By substituting these Fourier expansions into Eqs. (A2)–(A5), and defining column vectors $E=(\ldots,E_{ij,x},E_{ij,y},\ldots)^T$ and $H=(\ldots,H_{ij,x},H_{ij,y},\ldots)^T$, we can derive the following concise matrix form

$$\frac{\partial}{\partial z}E=T_1H,\quad \frac{\partial}{\partial z}H=T_2E. \tag{A8}$$

The matrices T_1 and T_2 are defined as

Downloaded 09 Apr 2013 to 171.67.34.205. This article is copyrighted as indicated in the abstract. Reuse of AIP content is subject to the terms at: http://jap.aip.org/about/rights_and_permissions

$$T_1^{ij;mn}=\frac{i}{k_0}\begin{pmatrix} k_{ij,x}\epsilon^{-1}_{ij;mn}k_{mn,y} & -k_{ij,x}\epsilon^{-1}_{ij;mn}k_{mn,x}+k_0^2\delta_{ij;mn} \\ k_{ij,y}\epsilon^{-1}_{ij;mn}k_{mn,y}-k_0^2\delta_{ij;mn} & -k_{ij,y}\epsilon^{-1}_{ij;mn}k_{mn,x}\end{pmatrix}, \tag{A9}$$

$$T_2^{ij;mn}=\frac{i}{k_0}\begin{pmatrix} -k_{ij,x}\delta_{ij;mn}k_{mn,y} & k_{ij,x}\delta_{ij;mn}k_{mn,x}-k_0^2\epsilon_{ij;mn} \\ -k_{ij,y}\delta_{ij;mn}k_{mn,y}+k_0^2\epsilon_{ij;mn} & k_{ij,y}\delta_{ij;mn}k_{mn,x}\end{pmatrix}, \tag{A10}$$

where $\epsilon_{ij;mn}=\epsilon_{i-m;j-n}$ and $\epsilon^{-1}_{ij;mn}=\epsilon^{-1}_{i-m;j-n}$ are Fourier coefficients.

From Eq. (A8) we obtain an eigenproblem for the electric field:

$$\frac{\partial^2}{\partial z^2}E=(T_1T_2)E=PE. \tag{A11}$$

Now suppose we used N_0 plane waves in the expansion, then T_1, T_2, and P are all $(2N_0)\times(2N_0)$ matrices. The solution of Eq. (A11) will give us $2N_0$ eigenvalues (denoted as β_i^2, $i=1,2,\ldots,2N_0$, with $\mathrm{Im}(\beta_i)\geqslant 0$) of the matrix $-P=-T_1T_2$. In addition, the $(2N_0)\times(2N_0)$ matrix S_a, whose j_{th} column is the eigenvector corresponding to the eigenvalue β_j^2, can also be obtained simultaneously. The eigenmode corresponding to β_i^2 is $E_i'(z)=E_{a,i}^+(z)+E_{a,i}^-(z)$, $E_{a,i}^+(z)=E_i^+e^{i\beta_i(z-z_{i-1})}$, $E_{a,i}^-(z)=E_i^-e^{-i\beta_i(z-z_{i-1})}$, where E_i^+ and E_i^- are both unknown variables. Further define column vector $\beta=(\ldots,\beta_i,\ldots)^T$, $E_a^+=[\ldots,E_{a,i}^+(z),\ldots]^T$, and $E_a^-=[\ldots,E_{a,i}^-(z),\ldots]^T$. The electric field column vector E is now expressed in the superposition of all the eigenmodes, $E=S_a(E_a^++E_a^-)$. The corresponding magnetic field column vector obtained from Eq. (A11): $H=T_1^{-1}\partial/\partial z\,E=T_1^{-1}S_a\partial/\partial z\,(E_a^++E_a^-)=iT_1^{-1}S_a\beta(E_a^+-E_a^-)=T_a(E_a^+-E_a^-)$, where $T_a=iT_1^{-1}S_a\beta$. It proves convenient to write the electric and magnetic fields at an arbitrary point inside the grating slice into a concise form:

$$\begin{pmatrix}E(z)\\H(z)\end{pmatrix}=\begin{pmatrix}S_a & S_a\\ T_a & -T_a\end{pmatrix}\begin{pmatrix}E_a^+(z)\\E_a^-(z)\end{pmatrix}. \tag{A12}$$

The EM fields in the two air films around the grating slice can also be solved in the same way, and the results have been expressed in Eqs. (3) and (4), but we can rewrite them in a way similar to Eq. (A12). Match of boundary conditions requests that all tangential field components of each plane wave be continuous at the two interfaces between the air films and the grating slice. At the left interface $z=z_{i-1}$:

$$\begin{pmatrix}S_0 & S_0\\ T_0 & -T_0\end{pmatrix}\begin{pmatrix}\Omega_{i-1}^+\\ \Omega_{i-1}^-\end{pmatrix}=\begin{pmatrix}S_a & S_a\\ T_a & -T_a\end{pmatrix}\begin{pmatrix}E_a^+(z_{i-1})\\ E_a^-(z_{i-1})\end{pmatrix}, \tag{A13}$$

while at the right interface $z=z_i$,

$$\begin{pmatrix}S_0 & S_0\\ T_0 & -T_0\end{pmatrix}\begin{pmatrix}\Omega_i^+\\ \Omega_i^-\end{pmatrix}=\begin{pmatrix}S_a & S_a\\ T_a & -T_a\end{pmatrix}\begin{pmatrix}E_a^+(z_i)\\ E_a^-(z_i)\end{pmatrix}, \tag{A14}$$

where S_0 and T_0 are counterparts of S_a and T_a in an air film. They can be analytically solved. Actually $S_0=I$, a unit matrix, T_0 is a block-diagonal matrix each block of which is a 2×2 matrix already given by $T_{0,ij}$ in Eq. (4). Notice that within the grating slice

$$\begin{pmatrix}E_a^+(z_i)\\ E_a^-(z_i)\end{pmatrix}=\begin{pmatrix}e^{i\beta h} & 0\\ 0 & e^{-i\beta h}\end{pmatrix}\begin{pmatrix}E_a^+(z_{i-1})\\ E_a^-(z_{i-1})\end{pmatrix}, \tag{A15}$$

where $h=z_i-z_{i-1}$ is the thickness of the slice, $e^{i\beta h}$ denotes a $(2N_0)\times(2N_0)$ diagonal matrix whose element is $e^{i\beta_i h}$, $i=1,2,\ldots,2N_0$. Deleting $[E_a^+(z_{i-1}),E_a^-(z_{i-1})]^T$ and $[E_a^+(z_i),E_a^-(z_i)]^T$ from Eqs. (A13)–(A15) yields

$$\begin{pmatrix}\Omega_i^+\\ \Omega_i^-\end{pmatrix}=\begin{pmatrix}a_{11} & a_{12}\\ a_{21} & a_{22}\end{pmatrix}^{-1}\begin{pmatrix}e^{i\beta h} & 0\\ 0 & e^{-i\beta h}\end{pmatrix}\begin{pmatrix}a_{11} & a_{12}\\ a_{21} & a_{22}\end{pmatrix}\times\begin{pmatrix}\Omega_{i-1}^+\\ \Omega_{i-1}^-\end{pmatrix}, \tag{A16}$$

where $a_{11}=\frac{1}{2}(S_a^{-1}S_0+T_a^{-1}T_0)$, $a_{12}=\frac{1}{2}(S_a^{-1}S_0-T_a^{-1}T_0)$, and $a_{21}=a_{12}$, $a_{22}=a_{11}$. Equation (A16) has already presented the T-matrix for slice i, namely,

$$T_i=\begin{pmatrix}t_{11}^i & t_{12}^i\\ t_{21}^i & t_{22}^i\end{pmatrix}=\begin{pmatrix}a_{11} & a_{12}\\ a_{21} & a_{22}\end{pmatrix}^{-1}\begin{pmatrix}e^{i\beta h} & 0\\ 0 & e^{-i\beta h}\end{pmatrix}\times\begin{pmatrix}a_{11} & a_{12}\\ a_{21} & a_{22}\end{pmatrix}. \tag{A17}$$

Now it becomes clear why the T-matrix formalism is numerically unstable for thick gratings (see the two phase factors $e^{i\beta h}$ and $e^{-i\beta h}$.) For those Bragg wave components where β_i has a significant imaginary part, one of them must be exponentially increased through the whole slab of gratings, rendering numerical instability such as overflow.

In principle, the S matrix can be calculated from the T matrix through a transformation that has already been stated in this article. However, we prefer to derive the S matrix for slice i directly from Eq. (A16) largely depending on analytical algebra. This proves to be more stable and reliable numerically. After some algebraic manipulations, we finally arrive at

$$s^i=\begin{pmatrix}s_{11}^i & s_{12}^i\\ s_{21}^i & s_{22}^i\end{pmatrix}=\begin{pmatrix}p_1t_1+p_2t_2 & p_1t_2+p_2t_1\\ p_1t_2+p_2t_1 & p_1t_1+p_2t_2\end{pmatrix}, \tag{A18}$$

where $p_1=[a_{11}-e^{i\beta h}a_{12}a_{11}^{-1}e^{i\beta h}a_{12}]^{-1}$, $p_2=a_{11}^{-1}e^{i\beta h}a_{12}[a_{11}-e^{i\beta h}a_{12}a_{11}^{-1}e^{i\beta h}a_{12}]^{-1}$, $t_1=e^{i\beta h}a_{11}$, and $t_2=-a_{12}$. From Eq. (A18), it is obvious that s^i is a block-symmetric matrix, reflecting the fact that the grating slice is symmetric with respect to its middle plane at $z=(z_{i-1}+z_i)/2$.

[1] E. Yablonovitch, Phys. Rev. Lett. **58**, 2059 (1987).
[2] J. D. Joannopoulos, P. R. Villeneuve, and S. Fan, Nature (London) **386**, 143 (1997).
[3] K. Sakoda, *Optical Properties of Photonic Crystals* (Springer, Berlin, 2001).

Downloaded 09 Apr 2013 to 171.67.34.205. This article is copyrighted as indicated in the abstract. Reuse of AIP content is subject to the terms at: http://jap.aip.org/about/rights_and_permissions

[4] *Electromagnetic Theory of Gratings*, edited by R. Petit (Springer, Berlin, 1980).
[5] M. G. Moharam and T. K. Gaylord, J. Opt. Soc. Am. **72**, 1385 (1982).
[6] M. G. Moharam, E. B. Grann, D. A. Pommet, and T. K. Gaylord, J. Opt. Soc. Am. A **12**, 1068 (1995).
[7] L. Li, J. Opt. Soc. Am. A **14**, 2758 (1997).
[8] L. Li, J. Opt. Soc. Am. A **13**, 1024 (1996).
[9] L. Li, J. Opt. Soc. Am. A **10**, 2581 (1993).
[10] J. B. Pendry, J. Mod. Opt. **41**, 209 (1994).
[11] P. M. Bell, J. B. Pendry, L. Marin Moreno, and A. J. Ward, Comput. Phys. Commun. **85**, 306 (1995).
[12] K. M. Ho, C. T. Chan, and C. M. Soukoulis, Phys. Rev. Lett. **65**, 3152 (1990).
[13] D. Cassagne, C. Jouanin, and D. Bertho, Phys. Rev. B **53**, 7134 (1996).
[14] Z. Y. Li, J. Wang, and B. Y. Gu, Phys. Rev. B **58**, 3721 (1998).
[15] Z. Y. Li, B. Y. Gu, and G. Z. Yang, Eur. Phys. J. B **11**, 65 (1999).
[16] K. M. Ho, C. T. Chan, C. M. Soukoulis, R. Biswas, and M. Sigalas, Solid State Commun. **89**, 413 (1994).
[17] S. Y. Lin, J. G. Fleming, D. L. Hetherington, B. K. Smith, R. Biswas, K. M. Ho, M. M. Sigalas, W. Zurbrzycki, S. R. Kurtz, and J. Bur, Nature (London) **394**, 251 (1998).

Downloaded 09 Apr 2013 to 171.67.34.205. This article is copyrighted as indicated in the abstract. Reuse of AIP content is subject to the terms at: http://jap.aip.org/about/rights_and_permissions